

Light Resonances and the Low- q^2 Bin of R_{K^*}

Wolfgang Altmannshofer^a, Michael J. Baker^b, Stefania Gori^a,
Roni Harnik^c, Maxim Pospelov^{d,e,g}, Emmanuel Stamou^f,
Andrea Thamm^g

^a*Department of Physics, University of Cincinnati, Cincinnati, OH 45221, USA*

^b*Physik-Institut, Universität Zürich, 8057 Zürich, Switzerland*

^c*Theoretical Physics Department, Fermilab, Batavia, IL 60510, USA*

^d*Department of Physics and Astronomy, University of Victoria, Victoria,
BC V8P 5C2, Canada*

^e*Perimeter Institute for Theoretical Physics, Waterloo, ON N2L 2Y5, Canada*

^f*Enrico Fermi Institute, University of Chicago, Chicago, IL 60637, USA*

^g*Theoretical Physics Department, CERN, 1211 Geneva, Switzerland*

November 22, 2017

Abstract

LHCb has reported hints of lepton-flavor universality violation in the rare decays $B \rightarrow K^{(*)}\ell^+\ell^-$, both in high- and low- q^2 bins. Although the high- q^2 hint may be explained by new short-ranged interactions, the low- q^2 one cannot. We thus explore the possibility that the latter is explained by a new light resonance. We find that LHCb's central value of R_{K^*} in the low- q^2 bin is achievable in a restricted parameter space of new-physics scenarios in which the new, light resonance decays preferentially to electrons and has a mass within approximately 10 MeV of the di-muon threshold. Interestingly, such an explanation can have a kinematic origin and does not require a source of lepton-flavor universality violation. A model-independent prediction is a narrow peak in the differential $B \rightarrow K^*e^+e^-$ rate close to the di-muon threshold. If such a peak is observed, other observables, such as the differential $B \rightarrow Ke^+e^-$ rate and R_K , may be employed to distinguish between models. However, if a low-mass resonance is not observed and the low- q^2 anomaly increases in significance, then the case for an experimental origin of the lepton-flavor universality violating anomalies would be strengthened. To further explore this, we also point out that, in analogy to J/ψ decays, e^+e^- and $\mu^+\mu^-$ decays of ϕ mesons can be used as a cross check of lepton-flavor universality by LHCb with 5 fb^{-1} of integrated luminosity.

1 Introduction

The gauge sector of the Standard Model (SM) exhibits exact flavor universality, which is only broken by the Yukawa couplings of the quarks and leptons with the Higgs boson. One of the best ways to test this property of the SM is to measure semi-leptonic neutral current decays of B mesons. In the SM, these decays are induced at one-loop level and are additionally suppressed by the Glashow–Iliopoulos–Maiani (GIM) mechanism. For these decays, observables that are sensitive to lepton-flavor universality (LFU) are ratios of decay rates to muons and electrons, i.e.,

$$R_M = \frac{\text{BR}(B \rightarrow M\mu^+\mu^-)}{\text{BR}(B \rightarrow Me^+e^-)}, \quad M = K, K^*, X_s, \dots \quad (1.1)$$

Recently, the LHCb collaboration determined [1, 2]

$$R_K \equiv \frac{\text{BR}(B \rightarrow K\mu^+\mu^-)}{\text{BR}(B \rightarrow Ke^+e^-)} = 0.745_{-0.074}^{+0.090} \pm 0.036, \quad \text{for } q^2 \in [1, 6] \text{ GeV}^2, \quad (1.2)$$

$$R_{K^*} \equiv \frac{\text{BR}(B \rightarrow K^*\mu^+\mu^-)}{\text{BR}(B \rightarrow K^*e^+e^-)} = \begin{cases} 0.66_{-0.07}^{+0.11} \pm 0.03, & \text{for } q^2 \in [0.045, 1.1] \text{ GeV}^2, \\ 0.69_{-0.07}^{+0.11} \pm 0.05, & \text{for } q^2 \in [1.1, 6] \text{ GeV}^2, \end{cases} \quad (1.3)$$

where q^2 is the di-lepton invariant mass squared. The SM predictions for these observables have small, percent-level uncertainties. Away from the di-muon threshold, $q^2 = 4m_\mu^2 \simeq 0.045 \text{ GeV}^2$, R_K^{SM} and $R_{K^*}^{\text{SM}}$ are 1 with high precision [3, 4]. $R_{K^*}^{\text{SM}}$ in the low- q^2 bin is slightly below 1, mainly due to phase space effects [4]:

$$R_K^{\text{SM}} = 1.00 \pm 0.01, \quad \text{for } q^2 \in [1, 6] \text{ GeV}^2, \quad (1.4)$$

$$R_{K^*}^{\text{SM}} = \begin{cases} 0.91 \pm 0.03, & \text{for } q^2 \in [0.045, 1.1] \text{ GeV}^2, \\ 1.00 \pm 0.01, & \text{for } q^2 \in [1.1, 6] \text{ GeV}^2. \end{cases} \quad (1.5)$$

These predictions are in some tension with the LHCb measurements in eqs. (1.2) and (1.3). Combining the errors in quadrature, one finds an $\sim 2.6\sigma$ tension in R_K , and an $\sim 2.4\sigma$ and $\sim 2.5\sigma$ tension in the two bins for R_{K^*} .

If the discrepancies between measurements and SM predictions are due to New Physics (NP) from four-fermion contact interactions, the ratio R_{K^*} is expected to have a non-trivial q^2 dependence. At low di-lepton invariant mass, the $B \rightarrow K^*\ell^+\ell^-$ rates are dominated by a $1/q^2$ enhanced photon contribution, which strongly dilutes NP effects in the low- q^2 bin. Model independent analyses [5–9] find that a NP contact interaction that explains R_K and R_{K^*} in the high- q^2 bins affects R_K^* in the low- q^2 bin typically by at most 10%. We are, therefore, led to explore the possibility that the low- q^2 discrepancy in R_{K^*} may be a hint for new light degrees of freedom, which cannot be described by an effective Lagrangian with only SM fields (see, however, also ref. [10]).

The possible effects of resonances below the electroweak scale on LFU in $B \rightarrow K^{(*)}\ell^+\ell^-$ have been previously considered in refs. [11–18]. In this work, we point out that a light, new resonance can affect the low- q^2 bin of R_{K^*} only in a very restricted

range of parameter space once all relevant constraints are taken into account. If the resonance has a mass significantly below the di-muon threshold, it affects R_{K^*} from an off-shell exchange. We find, however, that the related two-body decays of B mesons into final states containing the resonance on-shell typically oversaturate the total B width. We thus exclude such a scenario. If the resonance mass is close to or above the di-muon threshold, strong constraints exist from the existing measurements of the differential $B \rightarrow K^*e^+e^-$ rate [19] and from di-muon resonance searches in the $B \rightarrow K^*\mu^+\mu^-$ decay [20].

Our main result is that a light new resonance can produce a suppression of R_{K^*} in the low- q^2 bin only if the resonance decays preferentially to electrons and its mass is within approximately 10 MeV of the di-muon threshold. Such a situation can occur either because the resonance couples non-universally to charged leptons or because its decay to muons is kinematically forbidden even if its coupling is universal, e.g., dark-photon models. This leads to testable consequences for other LHCb measurements. In particular, it implies that the differential $B \rightarrow K^*e^+e^-$ rate close to the di-muon threshold features a peak that should be searched for experimentally. Analogously, the $B_s \rightarrow \phi e^+e^-$ spectrum has to feature a peak close to the di-muon threshold of the same relative size. A peak should also be present in the differential $B \rightarrow Ke^+e^-$ rate close to the di-muon threshold. While K^* and ϕ are vectors, K is a pseudoscalar. Therefore, the size of the peak in $B \rightarrow Ke^+e^-$ is model dependent and allows us to distinguish between different flavor violating interactions of the resonance to bottom and strange quarks.

The connection between the deviation in the low- q^2 bin of R_{K^*} and the peaks in the $B \rightarrow K^*e^+e^-$ and $B_s \rightarrow \phi e^+e^-$ spectra is robust. This allows us to further conclude that if the low- q^2 deviation persists and becomes statistically significant, but no peak is observed, the case for a systematic experimental origin of the deviation would be strengthened. This will have implications for the interpretation of any anomaly in the high- q^2 bin, if it persists.

The paper is organized as follows: In section 2, we show how a light, new resonance can affect the low- q^2 bin of R_{K^*} taking into account all relevant experimental constraints. This analysis is model-independent since it does not depend on how the resonance couples to bottom and strange quarks. We consider both off-shell and on-shell explanations and argue that only the latter is consistent with other observations. We also discuss the model-independent implications for the $B \rightarrow K^*e^+e^-$ and $B_s \rightarrow \phi e^+e^-$ spectra. In section 3, we consider several models, focusing on new vector resonances just below the di-muon threshold. We analyse different ways to couple the resonance to the flavor changing quark current and show the corresponding model dependent implications for the $B \rightarrow Ke^+e^-$ decay. In section 4, we propose additional LFU measurements for the LHCb experiment that could lead to further insights into the origin of the low- q^2 anomaly. Finally, in section 5 we discuss and summarize our results. In appendix A we elaborate on the off-shell case, and in appendix B we report the form factors used in our analysis.

2 Model-Independent Analysis

In this section, we discuss the impact of a light, new resonance, X , in R_{K^*} , keeping the discussion as model independent as possible.

2.1 Off-shell effect of a light resonance

The off-shell exchange of a resonance far below the di-muon threshold can in principle contribute to the $B \rightarrow K^* \ell^+ \ell^-$ rate in the low- q^2 bin. The propagator is approximately proportional to $1/q^2$, which enhances the off-shell contribution at low q^2 (like the SM photon). We thus expect such off-shell exchanges to have a high impact on measurements at low q^2 , which could account for the anomaly in the low- q^2 bin of R_{K^*} . However, we show here that such a setup is unlikely to satisfy existing experimental constraints.

To illustrate this point, we consider a very light resonance, X , with a mass far below the low- q^2 bin of R_{K^*} , i.e., $m_X^2 \ll 0.045 \text{ GeV}^2$, that couples to leptons (with coupling g_ℓ , $\ell = \mu, e$) and off-diagonally to bottom and strange quarks. If the off-shell exchange of X produces a visible effect in R_{K^*} , then this would typically imply a two-body inclusive $B \rightarrow X_s X$ width that exceeds the total B width. For example, if we assume that X has a flavor changing dipole interaction¹, we estimate that

$$\frac{\Gamma(B \rightarrow X_s X)}{\Gamma_{B,\text{tot}}^{\text{SM}}} \sim \frac{e^2}{4g_\ell^2} (\Delta R_{K^*})^2 \times \text{BR}(B \rightarrow X_s \gamma) \simeq 800\% \times \left(\frac{0.3 \cdot 10^{-3}}{g_\ell} \right)^2 \left(\frac{\Delta R_{K^*}}{0.3} \right)^2, \quad (2.1)$$

where $\Gamma_{B,\text{tot}}^{\text{SM}}$ is the total width of the B meson in the SM, $\Delta R_{K^*} \equiv R_{K^*}^{\text{SM}} - R_{K^*}$ (in the low- q^2 bin), and where we have used $\text{BR}(B \rightarrow X_s \gamma) = (3.32 \pm 0.15) \cdot 10^{-4}$ [21]. Given that the coupling of light (~ 10 's of MeV) new degrees of freedom to electrons and muons are constrained to be $\lesssim 10^{-3}$ (see fig. 7 in appendix A), the $B \rightarrow X_s X$ decay width typically exceeds the experimentally determined total B width by a factor of a few, which excludes such a scenario. For the derivation of eq. (2.1) we assumed that the resonance couples only to one type of lepton. Barring cancellations, the same argument leads to even more stringent constraints if we assume couplings to both muons and electrons. We quantify our argument in detail for a vector resonance in appendix A.

2.2 On-shell production of a light resonance

Having argued that the off-shell exchange of a light resonance cannot affect the low- q^2 bin of R_{K^*} in an appreciable way, we now discuss scenarios in which on-shell production of the resonance ($B \rightarrow K^* X$ with $X \rightarrow \ell^+ \ell^-$) affects the low- q^2 bin. In the case of a narrow resonance, this is possible as long as the mass of the resonance is inside the $[0.045, 1.1] \text{ GeV}^2$ bin, up to experimental resolution effects. In the on-shell approximation there is no interference with the SM $b \rightarrow s \ell \ell$ amplitudes, so the resonance can only enhance the $B \rightarrow K^* \ell^+ \ell^-$ rates. Therefore, in order to explain R_{K^*} in this scenario, the

¹The qualitative conclusions remain the same for different choices of the particle X and its interactions with fermions.

resonance has to decay more often into electrons than into muons, i.e., $\text{BR}(X \rightarrow e^+e^-) > \text{BR}(X \rightarrow \mu^+\mu^-)$.

In general, the scenario can be model independently defined by the following set of parameters: (i) the mass of the resonance, m_X ; (ii) the B meson branching ratio $\text{BR}(B \rightarrow K^*X)$; (iii) the leptonic branching ratios of the resonance, $\text{BR}(X \rightarrow e^+e^-)$ and $\text{BR}(X \rightarrow \mu^+\mu^-)$; (iv) the total width of the resonance Γ_{tot}^X .

We will find that the mass of X has to be close to the di-muon threshold. Far below the threshold, the effect in R_{K^*} becomes negligible, while far above the threshold the constraints from the measured $B \rightarrow K^*e^+e^-$ spectrum and searches for $B \rightarrow K^*X(\rightarrow \mu^+\mu^-)$ are severe. In the following, we therefore focus on the case of X masses for which the decay to τ 's or to two or more hadrons is kinematically forbidden. The total X width is then the sum of the partial width into the visible final states of electrons and muons, as well as the width into invisible final states like neutrinos and any other kinematically accessible decay channel of the X to “dark”, non-SM particles.² We work in the limit of narrow width, $\Gamma_{\text{tot}}^X \ll m_X$. The width of X is bounded from below, as the leptons and the K^* are observed to originate from the same vertex [2]. Demanding that the X decays promptly ($c\tau \lesssim 2\text{mm}$) and using a typical boost factor of 200,³ we find $\Gamma_{\text{tot}}^X \gtrsim 0.02$ eV. This is compatible with the narrow-width assumption for the range of masses we consider.

The new resonance then affects the $B \rightarrow K^*\ell^+\ell^-$ branching ratios in a given bin of di-lepton invariant mass $[q_{\text{min}}^2, q_{\text{max}}^2]$ in the following way

$$\langle \text{BR}_{\ell\ell} \rangle \Big|_{q_{\text{min}}}^{q_{\text{max}}} = \langle \text{BR}_{\ell\ell}^{\text{SM}} \rangle \Big|_{q_{\text{min}}}^{q_{\text{max}}} + \text{BR}(B \rightarrow K^*X) \cdot \text{BR}(X \rightarrow \ell^+\ell^-) \cdot \mathcal{G}^{(r_\ell)}(q_{\text{min}}, q_{\text{max}}). \quad (2.2)$$

The function $\mathcal{G}^{(r_\ell)}(q_{\text{min}}, q_{\text{max}})$ models the imperfect di-lepton mass resolution of the LHCb detector. We assume a Gaussian smearing such that

$$\mathcal{G}^{(r_\ell)}(q_{\text{min}}, q_{\text{max}}) = \frac{1}{\sqrt{2\pi}r_\ell} \int_{q_{\text{min}}}^{q_{\text{max}}} d|q| e^{-\frac{(|q|-m_X)^2}{2r_\ell^2}}. \quad (2.3)$$

For the resolutions we use $r_e = 10$ MeV for electrons [23] and $r_\mu = 2$ MeV for muons [24]. We neglect the dependence of the mass resolution on q^2 , as we always consider a very narrow range of masses for X .

The NP prediction for R_{K^*} in the bin $[q_{\text{min}}^2, q_{\text{max}}^2]$ is then determined by the corresponding modified branching ratios

$$R_{K^*} = \langle \text{BR}_{\mu\mu} \rangle \Big|_{q_{\text{min}}}^{q_{\text{max}}} / \langle \text{BR}_{ee} \rangle \Big|_{q_{\text{min}}}^{q_{\text{max}}}. \quad (2.4)$$

We use `flavio` [25] to compute the SM predictions and uncertainties of R_{K^*} and the branching ratios $\langle \text{BR}_{\ell\ell}^{\text{SM}} \rangle \Big|_{q_{\text{min}}}^{q_{\text{max}}}$.

As long as the mass of the new resonance is not more than $\mathcal{O}(r_e) = \mathcal{O}(10$ MeV) outside the lower edge of the $[0.045, 1.1]$ GeV² bin, the $B \rightarrow K^*X$ and $X \rightarrow \ell^+\ell^-$ branching

²We do not consider the decay $X \rightarrow \pi_0\gamma$, which has a tiny branching ratio in typical models. We also do not consider the decay $X \rightarrow \gamma\gamma$ that is possible if X is a (pseudo)scalar.

³We estimate the boost factor using a mean energy of 80 GeV for the B mesons at LHCb [22].

ratios can be adjusted to account for the R_{K^*} value measured by LHCb. Various other measurements constrain the NP parameter space. The most stringent constraints are:

- The LHCb search for a resonance in the di-muon invariant mass spectrum in the $B \rightarrow K^*X(\rightarrow \mu^+\mu^-)$ decay [20]. This search places very stringent upper limits on the product $\text{BR}(B \rightarrow K^*X) \times \text{BR}(X \rightarrow \mu^+\mu^-)$, which are given as a function of the X mass and the X width. If X is to explain the low- q^2 bin of R_{K^*} , the bounds for a promptly decaying X apply. No bound can be obtained from this search for $m_X < 2m_\mu$, where $\text{BR}(X \rightarrow \mu^+\mu^-) = 0$.
- The differential branching ratio of $B \rightarrow K^*e^+e^-$ measured by LHCb [19] constrains the product of $\text{BR}(B \rightarrow K^*X) \times \text{BR}(X \rightarrow e^+e^-)$ for resonance masses below and above the di-muon threshold. LHCb presents measurements of six bins of q^2 , ranging from 0.0004 GeV² to 1 GeV² [19]. Interestingly, a small excess of $B \rightarrow K^*e^+e^-$ events is observed in the q^2 bin below the di-muon threshold, leading to a slight preference for a non-zero $\text{BR}(B \rightarrow K^*X) \times \text{BR}(X \rightarrow e^+e^-)$ for $m_X < 2m_\mu$.
- The bounds on $\text{BR}(B \rightarrow K^*\nu\bar{\nu})$ obtained at the B factories [26, 27] are relevant for the case in which the resonance has a sizeable branching ratio into invisible final states. The most stringent bound is obtained by Belle [26]; it reads $\text{BR}(B \rightarrow K^*X) \times \text{BR}(X \rightarrow \text{invisible}) < 5.5 \cdot 10^{-5}$ at 90% Confidence Level (C.L.).

For the numerical analysis, we construct a χ^2 function based on a gaussian likelihood function that contains the low- q^2 bin of R_{K^*} , the limits from the $B \rightarrow K^*X(\rightarrow \mu^+\mu^-)$ search, the $B \rightarrow K^*e^+e^-$ distribution, and the $B \rightarrow K^*\nu\bar{\nu}$ bound. To account for the asymmetric error of R_{K^*} we use the positive (negative) side of error if the R_{K^*} prediction lies above (below) the experimental central value. From ref. [20] we extract the bound on prompt X decays $\text{BR}(B \rightarrow K^*X) \times \text{BR}(X \rightarrow \mu^+\mu^-) < 3 \cdot 10^{-9}$ at 95% C.L., which we implement in the χ^2 for all masses $m_X > 2m_\mu$ close to the di-muon threshold. We take into account all q^2 bins measured in the LHCb analysis [19] of $B \rightarrow K^*e^+e^-$. The theory uncertainties in this q^2 region are mainly due to form factors and CKM elements. We, therefore, assume that these uncertainties are 90% correlated across the bins. Efficiency effects are estimated by comparing the SM prediction from `flavio` with the ones presented in the LHCb analysis [19]. To capture possible uncertainties of this procedure, we inflate the theory uncertainties from `flavio` by a factor of 1.5 to be conservative. Taking into account the correlation, we add the theory errors in quadrature with the experimental errors. We have checked that choosing a different level of correlation in the theory uncertainties does not lead to qualitative changes in our results.

For a given set of NP parameters, we plot contours of $\Delta\chi^2 = \chi^2 - \chi_{\min}^2$ corresponding to the preferred regions at 68.27% and 95.45% C.L., and give both χ_{\min}^2 and χ_{SM}^2 for comparison. We also show separately the preferred 68.27% C.L. region for R_{K^*} in the low- q^2 bin ignoring all constraints. For the constraints from $B \rightarrow K^*X(\rightarrow \mu^+\mu^-)$, $B \rightarrow K^*e^+e^-$, and $B \rightarrow K^*\nu\bar{\nu}$ we shade the part of the parameter space that is excluded at 95% C.L. We find that once the above mentioned constraints are taken into account,

Dark photon

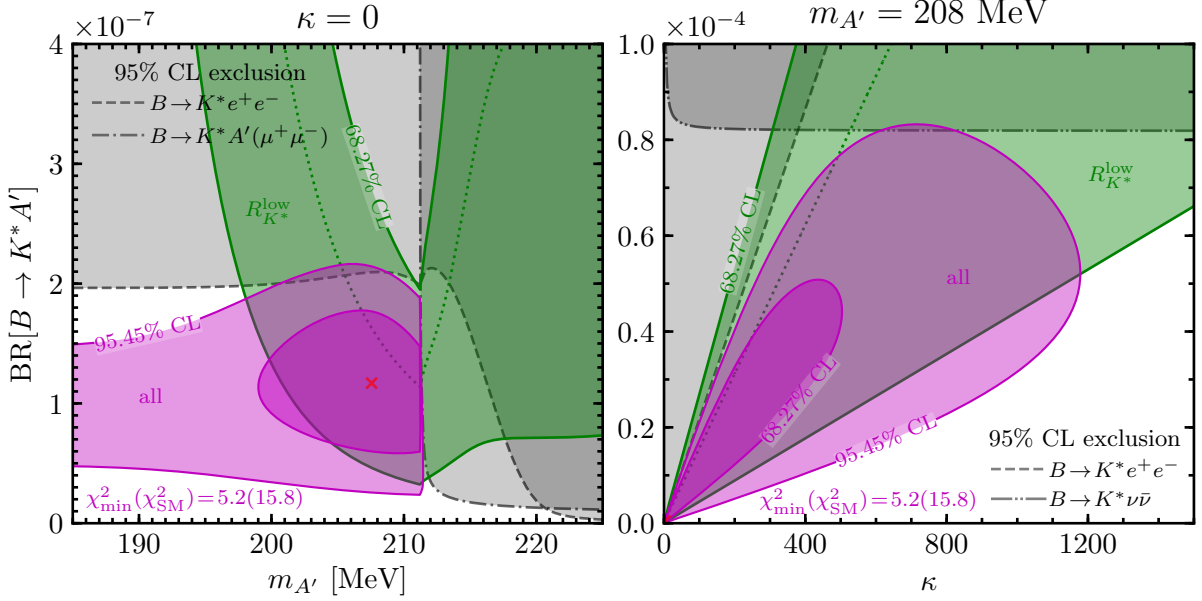


Figure 1: Preferred regions of parameter space for a dark-photon explanation of the low- q^2 bin of R_{K^*} . In the left plot, the dark photon is assumed to decay 100% to electrons and muons; the dark-photon mass and $\text{BR}(B \rightarrow K^* A')$ are varied. In the right plot, the dark-photon mass is fixed to $m_{A'} = 208$ MeV; the $\text{BR}(B \rightarrow K^* A')$ and the invisible width (parameterized by κ , see text) are varied. The red cross at $\text{BR}(B \rightarrow K^* A') = 1.2 \cdot 10^{-7}$ and $m_{A'} = 208$ MeV (left), and $\text{BR}(B \rightarrow K^* A') = 1.2 \cdot 10^{-7}$ and $\kappa = 0$ (right) are the best-fit values in each case.

the discrepancy in the low- q^2 bin of R_{K^*} can only be addressed in a very restricted range of NP parameter space. We first illustrate this in a simple benchmark scenario, in which we identify the resonance with a dark photon, i.e., $X \Rightarrow A'$. We then discuss the viable parameter space in the case of a generic resonance.

2.2.1 Dark photon – LFU violation without LFU violation

If the resonance is a dark photon, A' , its branching ratios to electrons and muons are fixed by the dark-photon mass, $m_{A'}$, its total width, $\Gamma_{\text{tot}}^{A'}$, and either the kinetic-mixing parameter ϵ or equivalently the dark-photon partial width to non-SM particles, $\Gamma_{\text{other}}^{A'}$. In the mass range we consider, the total width is given by

$$\Gamma_{\text{tot}}^{A'} = \Gamma_{ee}^{A'} + \Gamma_{\mu\mu}^{A'} + \Gamma_{\text{other}}^{A'}, \quad (2.5)$$

with

$$\Gamma_{\ell\ell}^{A'} = \epsilon^2 \frac{e^2}{12\pi} m_{A'} \left(1 + 2 \frac{m_\ell^2}{m_{A'}^2} \right) \sqrt{1 - 4 \frac{m_\ell^2}{m_{A'}^2} \theta(m_{A'}^2 - 4m_\ell^2)}. \quad (2.6)$$

We find it convenient to parameterize $\Gamma_{\text{other}}^{A'} = \kappa(\Gamma_{ee}^{A'} + \Gamma_{\mu\mu}^{A'})$. In this parametrization, the dark-photon branching ratios to electrons and muons are independent of ϵ . A dark-

photon benchmark is then fully specified by choosing⁴

$$m_{A'}, \quad \text{BR}(B \rightarrow K^* A'), \quad \kappa. \quad (2.7)$$

In the left panel of fig. 1 we consider the case of $\kappa = 0$ and show the constraints and preferred region in the parameter space of $m_{A'}$ and $\text{BR}(B \rightarrow K^* A')$. In green we show the preferred 68.27% C.L. region for the low- R_{K^*} bin and in magenta the preferred 68.27% and 95.45% C.L. regions of the combined χ^2 . LHCb's constraints on $B \rightarrow K^* e^+ e^-$ and $B \rightarrow K^* X (\rightarrow \mu^+ \mu^-)$ exclude the shaded grey regions at 95% C.L. There is no constraint from $B \rightarrow K^* \nu \bar{\nu}$ here since $\kappa = 0$. The best-fit point of the joint χ^2 is at $m_{A'} \simeq 208$ MeV and $\text{BR}(B \rightarrow K^* A') \simeq 1.2 \cdot 10^{-7}$ (red cross in fig. 1).⁵ We see that the preferred region (magenta) is constrained to be below and close to the di-muon threshold. After profiling away the $\text{BR}(B \rightarrow K^* A')$ direction we find that $m_{A'} \in [203, 211]$ MeV at 68.27% C.L. The comparison of the minimum of the joint χ^2 , $\chi_{\text{min}}^2 = 5.2$, to the SM one, $\chi_{\text{SM}}^2 = 15.8$, shows that a dark photon in the preferred region describes low- q^2 data significantly better than the SM alone. This is driven by an improved fit to R_{K^*} .

Next we turn on the partial width of A' to light non-SM particles, i.e., $\kappa \neq 0$. The presence of these additional decay channels reduces the branching ratios of A' to electrons and muons. Correspondingly, a larger $\text{BR}(B \rightarrow K^* A')$ is required to explain the anomaly. This is illustrated in the right panel of fig. 1 where we fix the dark-photon mass to $m_{A'} = 208$ MeV and show the preferred region of parameter space in the κ vs. $\text{BR}(B \rightarrow K^* A')$ plane. We see that for large values of $\kappa > \mathcal{O}(10^3)$, the constraint from $B \rightarrow K^* + \text{invisible}$ excludes an explanation of R_{K^*} by the dark photon. However, the point with $\kappa = 0$ is slightly preferred.

Interestingly, the dark-photon explanation of the low- q^2 bin does not introduce any sources of LFU violation beyond the SM. In this attractive, minimal scenario, the modification of R_{K^*} arises due to the difference of electron and muon mass. Note that the value of R_{K^*} does not depend on the kinetic-mixing parameter, ϵ , as long as the dark photon decays promptly. At a mass of ~ 210 MeV the dark photon is constrained by the APEX, MAMI, and BaBar experiments to have a mixing $\epsilon \lesssim 10^{-3}$ [28–32]. A dark photon with a coupling that saturates this limit has a decay length of about 80 microns including a typical Lorentz boost factor of 200 (see footnote 3). This is fully compatible with the maximal displacement of 2 mm seen in the R_{K^*} measurement [2].

2.2.2 Generic resonance

In the generic case, we treat the electron and muon branching ratios of the resonance as independent parameters. Instead of introducing a Lagrangian, for which we would have to specify the spin of the resonance and the chiral structure of its couplings, we introduce

⁴The kinetic mixing parameter ϵ determines the total width of the dark photon. As long as ϵ is large enough such that the dark photon decays promptly, the exact value of ϵ is not relevant for our discussion.

⁵For comparison, note that in the SM the branching ratios in the low- q^2 bin are $\langle \text{BR}_{ee}^{\text{SM}} \rangle|_{\text{low-}q^2} \simeq 1.3 \cdot 10^{-7}$ and $\langle \text{BR}_{\mu\mu}^{\text{SM}} \rangle|_{\text{low-}q^2} \simeq 1.2 \cdot 10^{-7}$.

Generic resonance, X , with $m_X = 220$ MeV

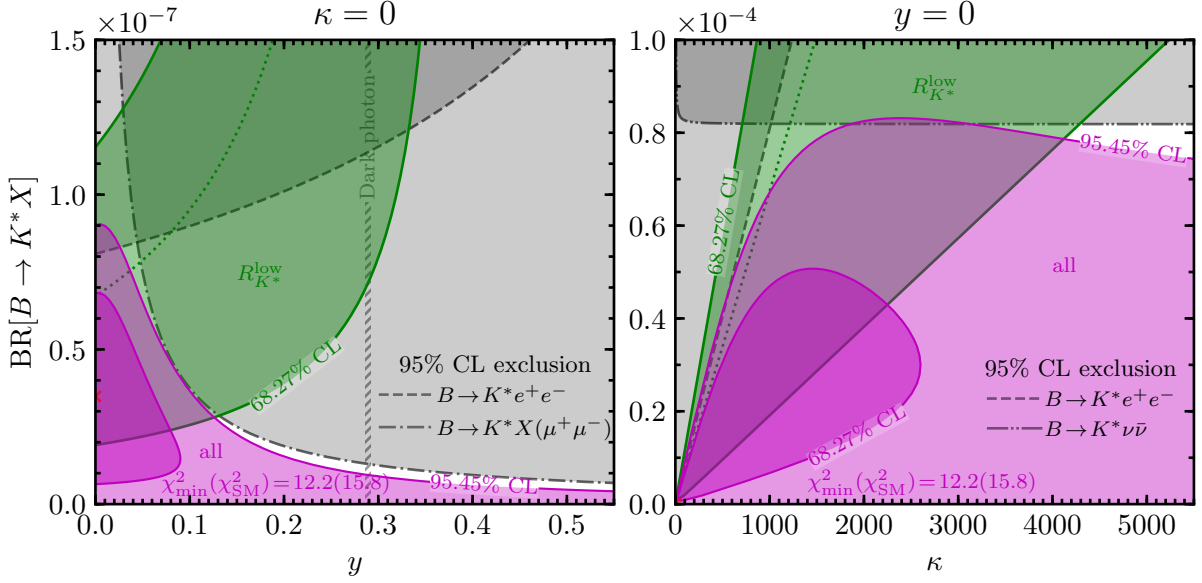


Figure 2: Preferred regions of parameter space for a generic resonance explanation of the low- q^2 bin of R_{K^*} . The mass of the resonance is fixed to 220 MeV. In the left plot the invisible branching ratio is set to zero ($\kappa = 0$). In the right plot the branching ratio to muons is set to zero ($y = 0$). The red crosses at $\text{BR}(B \rightarrow K^* X) = 3.5 \cdot 10^{-8}$ and $y = 0$ (left), and $\text{BR}(B \rightarrow K^* X) = 3.5 \cdot 10^{-8}$ and $\kappa = 0$ (right) correspond to the best-fit values.

the parameter $y \in [0, 1]$ which interpolates between the case of $\text{BR}(X \rightarrow \mu^+ \mu^-) = 0$ for $y = 0$ and $\text{BR}(X \rightarrow e^+ e^-) = 0$ for $y = 1$. We thus use the parameterization

$$\text{BR}(X \rightarrow e^+ e^-) = \frac{1}{1 + \kappa} \cdot (1 - y), \quad (2.8)$$

$$\text{BR}(X \rightarrow \mu^+ \mu^-) = \frac{1}{1 + \kappa} \cdot y, \quad (2.9)$$

$$\text{BR}(X \rightarrow \text{other}) = \frac{\kappa}{1 + \kappa}. \quad (2.10)$$

The generic scenario is then fully specified by the parameter set

$$m_X, \quad \text{BR}(B \rightarrow K^* X), \quad y, \quad \kappa. \quad (2.11)$$

For a resonance mass below the di-muon threshold, i.e., $m_X < 2m_\mu$, the branching ratio to muons vanishes and, thus, at these masses this scenario is identical to the dark-photon model discussed in the previous section. In fig. 2 we pick a mass for the resonance above the di-muon threshold, $m_X = 220$ MeV. In the left panel, we show the preferred region in the space of $\text{BR}(B \rightarrow K^* X)$ and y , fixing $\kappa = 0$ corresponding to the case of no invisible decays. We observe that a resonance with a larger branching ratio to electrons than to muons, i.e., $y < 0.5$, is preferred. The dashed vertical line at $y = 0.29$

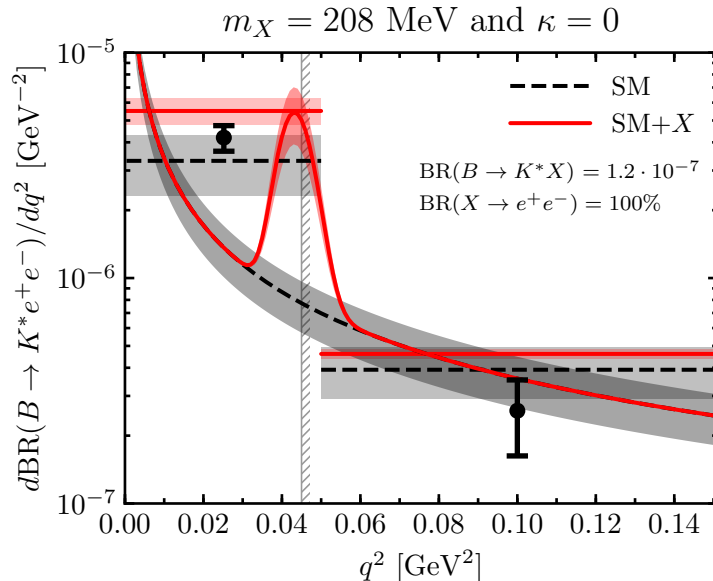


Figure 3: The differential branching ratio $d\text{BR}(B \rightarrow K^* e^+ e^-)/dq^2$ in the SM (dashed black) and in the presence of a resonance with the best-fit values for its mass and $\text{BR}(B \rightarrow K^* X)$ (solid red). We also show the binned predictions together with the LHCb measurements from ref. [19]. The vertical line indicates the lower boundary of the low- q^2 bin in the R_{K^*} measurement.

corresponds to the case of the dark-photon scenario discussed above. In the right panel, we vary $\text{BR}(B \rightarrow K^* X)$ and κ , fixing $y = 0$ corresponding to $\text{BR}(X \rightarrow \mu^+ \mu^-) = 0$. As in the case of the dark photon, a large invisible branching ratio is allowed.

We see that for $m_X = 220 \text{ MeV}$, the minimum of the total χ^2 is significantly larger than for the dark-photon case above ($\chi^2_{\text{min}} = 12.2$ and 5.2 , respectively) and corresponds to $\text{BR}(B \rightarrow K^* X) = 3.5 \cdot 10^{-8}$ and $y = 0$ in the case of $\kappa = 0$, and to $\text{BR}(B \rightarrow K^* X) = 3.5 \cdot 10^{-8}$ and $\kappa = 0$ in the case of $y = 0$ (red crosses in fig. 2). This is predominantly due to the tension between the low- q^2 bin in R_{K^*} and the $B \rightarrow K^* e^+ e^-$ constraint for this choice of m_X . If we increase the X mass to values above 220 MeV , the constraint from the $B \rightarrow K^* e^+ e^-$ spectrum becomes stronger excluding an explanation of the low- q^2 anomaly in R_{K^*} .

2.2.3 Model-independent predictions

As discussed above, any on-shell explanation of the low- q^2 bin of R_{K^*} requires a resonance close to the di-muon threshold decaying preferentially into electrons.⁶ A model-

⁶ In the past, a new particle in a very similar mass range had been proposed in connection with flavor physics. A light unspecified resonance was invoked as an explanation for the anomalous clustering of events with di-muon mass at $214.3 \pm 0.5 \text{ MeV}$ in the $\Sigma^+ \rightarrow p \mu^+ \mu^-$ decay by the HyperCP collaboration [33]. Recent LHCb measurements of the same decay mode do not lend further support to a hypothesis of a new 214 MeV particle [34]. A translation of these results to the B -meson case

independent key prediction is therefore a peak in the differential $B \rightarrow K^*e^+e^-$ rate at a q^2 close to the di-muon threshold. For a resonance that decays only to electrons ($y = 0, \kappa = 0$), the 68.27% C.L. region for the mass is $m_X \in [203, 212]$ MeV. If instead the resonance has a non-negligible decay mode into muons (like the dark photon) the 68.27% C.L. region is $m_X \in [203, 211]$ MeV.

For a resonance mass below the di-muon threshold, the size of the peak is completely fixed. Above the di-muon threshold the size of the peak scales as $\text{BR}(X \rightarrow e^+e^-)/(\text{BR}(X \rightarrow e^+e^-) - \text{BR}(X \rightarrow \mu^+\mu^-))$. In fig. 3 we show the peak for the best fit point below the di-muon threshold for $\kappa = 0$. We calculate the SM rate using `flavio`. We see that the SM rate rises as $q^2 \rightarrow 0$, due to the contribution from the photon pole. We assume that the resonance is narrow and that the spread in the NP events comes from the experimental resolution in electron reconstruction. Even taking this into account, the peak still rises prominently above the background. Also shown in the plot are SM and NP predictions of $\text{BR}(B \rightarrow K^*e^+e^-)$ for the q^2 bins measured by LHCb [19] together with the experimental results. More data and a finer q^2 binning should resolve the peak if it is present. An analogous peak with the same relative size is predicted in the $B_s \rightarrow \phi e^+e^-$ decay.

3 Model-Dependent Implications

We now consider possible operators that could induce the $B \rightarrow K^*X$ transition for the case in which X is a generic vector resonance, i.e., $X \Rightarrow V$. In addition to constraining the Wilson coefficients, this will allow us to make predictions for other observables, i.e., the differential rate of $B \rightarrow Ke^+e^-$ and R_K . We shall find that a future precise measurement of the differential $B \rightarrow Ke^+e^-$ rate and of R_K at low q^2 can distinguish the different operators if they are responsible for the anomalous measurement of R_{K^*} in the low- q^2 bin.

We concentrate here on vector resonances with masses just below the di-muon threshold, such that the branching ratio into di-muons is zero. We assume 100% branching ratio into prompt electrons, neglecting possible decays into a dark sector or neutrinos. As we have shown in fig. 1, in the presence of a non-negligible invisible width of the resonance, a larger $B \rightarrow K^*V$ branching ratio and, therefore, larger couplings to quarks are required to compensate for the reduced $V \rightarrow e^+e^-$ branching ratio.

We consider flavor-violating couplings of the vector to bottom and strange quarks up to dimension six

$$\mathcal{L}_{\text{eff}} = \sum_{d=4,5,6} \left(\frac{C_{(d)}}{\Lambda^{d-4}} Q_{(d)} + \frac{C'_{(d)}}{\Lambda^{d-4}} Q'_{(d)} \right) + \text{h.c.}, \quad (3.1)$$

is not possible in a model-independent way.

where the operators are given by

$$Q_{(4)} = (\bar{s}_L \gamma_\mu b_L) V^\mu, \quad Q'_{(4)} = (\bar{s}_R \gamma_\mu b_R) V^\mu, \quad (3.2)$$

$$Q_{(5)} = (\bar{s}_L \sigma_{\mu\nu} b_R) V^{\mu\nu}, \quad Q'_{(5)} = (\bar{s}_R \sigma_{\mu\nu} b_L) V^{\mu\nu}, \quad (3.3)$$

$$Q_{(6)} = (\bar{s}_L \gamma_\mu b_L) \partial_\nu V^{\mu\nu}, \quad Q'_{(6)} = (\bar{s}_R \gamma_\mu b_R) \partial_\nu V^{\mu\nu}, \quad (3.4)$$

with $V_{\mu\nu} = \partial_\mu V_\nu - \partial_\nu V_\mu$. In eq. (3.1), we also included the primed operators with a coupling of opposite chirality with respect to the non-primed operators. The widths and the analysis presented here for the primed operators are equivalent to the ones of the corresponding non-primed operators. We thus refrain from explicitly showing the results for the primed operators. In what follows, we shall assume that only one Wilson coefficient contributes at a time. The presence of more than one operator may produce additional interference effects.

Note that if one restricts to processes involving on-shell V , even this minimal set of operators is over-complete. In particular, the free equation of motion for V relates $Q_{(6)} = m_V^2 Q_{(4)}$ and $Q'_{(6)} = m_V^2 Q'_{(4)}$. Nevertheless, these operators are not fully equivalent as the amplitudes with off-shell V exchange differ for $Q_{(4)}$ and $Q_{(6)}$. One can also wonder how a direct coupling of the vector to the bs current in $Q_{(4)}$ and $Q'_{(4)}$ is possible. Recent studies have shown that these interactions do indeed arise in models where a light V couples to quark currents that are not conserved when the SM mass terms and/or quantum anomaly effects are taken into account [35, 36]. Models with direct flavour-universal couplings of V to axial-vector current of quarks tend to develop $Q_{(4)}$ at one loop, while models with coupling of V to any linear combinations of lepton and baryon currents other than $B - L$ induce $Q_{(4)}$ at the two-loop level.

In concrete UV completions, the Wilson coefficients in eq. (3.1) will be suppressed by loop factors and couplings. To make a connection to such UV models we pick a set of assumptions motivated by concrete examples and define a rescaled $\tilde{C}_{(d)}$ for each $C_{(d)}$ as follows.

For $Q_{(4)}$ we assume that the interaction is induced by the couplings of the vector to anomalous currents in which case the coupling is two-loop suppressed [35] and we have

$$C_{(4)} = V_{tb} V_{ts}^* \left(\frac{e^2}{16\pi^2} \right)^2 \tilde{C}_{(4)}. \quad (3.5)$$

The concrete model of ref. [35] is gauged baryon number with a gauge coupling g_X and with a small kinetic mixing of the $U(1)_B$ and the photon. The translation from our coupling \tilde{C}_4 to this model is $\tilde{C}_{(4)} = \frac{3}{\sin^4 \theta_W} F \left(\frac{m_t^2}{m_W^2} \right) g_X \sim 10^2 g_X$, where $F(x)$ is a loop function of order one defined in [35]. In other classes of models, this coupling can be induced at one-loop [36], or at tree-level [37, 38].

For $Q_{(5)}$ and $Q_{(6)}$ we assume that as in the SM the relevant couplings are one-loop suppressed and that Minimal Flavor Violation aligns the flavor structure of the couplings

with the corresponding photonic operators in the SM:

$$\frac{C_{(5)}}{\Lambda} = \frac{4G_F}{\sqrt{2}} V_{tb} V_{ts}^* \frac{e^2}{16\pi^2} \frac{m_b}{e} \tilde{C}_{(5)} \frac{m_W^2}{\tilde{\Lambda}^2}, \quad (3.6)$$

$$\frac{C_{(6)}}{\Lambda^2} = \frac{4G_F}{\sqrt{2}} V_{tb} V_{ts}^* \frac{e^2}{16\pi^2} \frac{1}{e} \tilde{C}_{(6)} \frac{m_W^2}{\tilde{\Lambda}^2}. \quad (3.7)$$

Setting $\tilde{\Lambda} = m_W$ gives a Lagrangian in the normalization most frequently employed for the effective Lagrangian in the SM.⁷

3.1 Model interpretations of $B \rightarrow K^*$ data

The decay width $\Gamma(B \rightarrow K^*V)$ induced by each of the operators in eq. (3.1) is

$$\Gamma(B \rightarrow K^*V)|_{Q_{(4)}} = \frac{1}{64\pi} |C_{(4)}|^2 \frac{m_B^5}{m_V^2 m_{K^*}^2} \left(1 - \frac{m_{K^*}^2}{m_B^2}\right)^{-2} \sqrt{\lambda} \mathcal{F}_1\left(\frac{m_{K^*}^2}{m_B^2}, \frac{m_V^2}{m_B^2}\right), \quad (3.8)$$

$$\Gamma(B \rightarrow K^*V)|_{Q_{(5)}} = \frac{1}{64\pi} \frac{|C_{(5)}|^2}{\Lambda^2} \frac{m_B^5}{m_{K^*}^2} \left(1 - \frac{m_{K^*}^2}{m_B^2}\right)^{-2} \sqrt{\lambda} \mathcal{F}_2\left(\frac{m_{K^*}^2}{m_B^2}, \frac{m_V^2}{m_B^2}\right), \quad (3.9)$$

$$\Gamma(B \rightarrow K^*V)|_{Q_{(6)}} = \frac{1}{64\pi} \frac{|C_{(6)}|^2}{\Lambda^4} \frac{m_B^5 m_V^2}{m_{K^*}^2} \left(1 - \frac{m_{K^*}^2}{m_B^2}\right)^{-2} \sqrt{\lambda} \mathcal{F}_1\left(\frac{m_{K^*}^2}{m_B^2}, \frac{m_V^2}{m_B^2}\right), \quad (3.10)$$

where we have defined the kinematical function

$$\lambda \equiv 1 + \frac{m_{K^*}^4}{m_B^4} + \frac{m_V^4}{m_B^4} - 2 \frac{m_{K^*}^2}{m_B^2} - 2 \frac{m_V^2}{m_B^2} - 2 \frac{m_{K^*}^2 m_V^2}{m_B^2 m_B^2}, \quad (3.11)$$

and used $B \rightarrow K^*$ form factors from ref. [39] to compute \mathcal{F}_1 and \mathcal{F}_2 (see eqs. (B.3) and (B.4) in appendix B).

Analogous expressions hold for the $C'_{(d)}$ coefficients. Notice that the same combination of form factors enter the decay induced by $Q_{(4)}$ and $Q_{(6)}$.

We perform the χ^2 fit outlined in the previous section, including the constraints from $B \rightarrow K^*V(\rightarrow \mu^+\mu^-)$, $B \rightarrow K^*e^+e^-$ and from the measured value of R_{K^*} in the low- q^2 bin. In table 1, we list the best-fit value of the Wilson coefficients, having fixed $\Lambda = 1$ TeV, and vice versa the value of Λ having fixed the Wilson coefficient to be one. This is shown both for $C_{(d)}$ and the rescaled $\tilde{C}_{(d)}$.

We can now interpret the results of our best fit for the $\tilde{C}_{(d)}$ in table 1 in the context of UV models, as well as in connection with the high- q^2 bin of R_{K^*} .

- The dimension-four operators that can account for the low- q^2 anomaly are well-behaved perturbative models, even if the coupling is suppressed by two loops as in eq. (3.5). It is notable that in the model of gauged baryon number [36] this is achieved without any flavor violation neither in the quark nor the lepton sector, the former being generated by the CKM matrix and the latter by phase space.

⁷To see this for $Q_{(6)}$, use the equation of motion for V to relate $Q_{(6)}$ to the semileptonic vector four-fermion operator appearing in the SM (O_9).

| d | $C_{(d)}^{\text{best fit}} _{\Lambda=1 \text{ TeV}}$ | $\Lambda^{\text{best fit}} _{C_{(d)}=1}$ | $\tilde{C}_{(d)}^{\text{best fit}} _{\tilde{\Lambda}=1 \text{ TeV}}$ | $\tilde{\Lambda}^{\text{best fit}} _{\tilde{C}_{(d)}=1}$ |
|-----|--|--|--|--|
| 4 | $1.6 \cdot 10^{-10}$ | — | $1.0 \cdot 10^{-2}$ | — |
| 5 | $2.4 \cdot 10^{-7}$ | $4.1 \cdot 10^6 \text{ TeV}$ | 3.3 | 0.55 TeV |
| 6 | $3.7 \cdot 10^{-3}$ | 16 TeV | $2.1 \cdot 10^2$ | 69 GeV |

Table 1: Values for Wilson coefficients and NP at the best-fit point. For each operator the best-fit mass of the new resonance is approximately 208 MeV. The normalization of the Wilson coefficients $\tilde{C}_{(d)}$ is defined in eqs. (3.5)–(3.7).

- The dimension-five, dipole-type operators can fit the low- q^2 deviation for a NP at the TeV scale that is perturbative (coupling of order one) and respects Minimal Flavor Violation. Note that the same can be said for explanations of the high- q^2 deviation of R_{K^*} . Turning this statement around, a generic TeV-scale explanation of the high- q^2 anomaly can be augmented by a light mediator, for instance a dark photon, with a judiciously chosen mass in order to explain the low- q^2 anomaly as well.
- The dimension-six interpretation of the low- q^2 anomaly appears to be disfavored with our UV assumptions as a non-perturbative coupling is required if the scale of NP is at the electroweak scale or higher.

Existing data does not further constrain the parameter space of the models we discussed. Current experiments, however, can test and distinguish these models.

3.2 Predictions for $B \rightarrow K$ data

Equipped with specific models we can now correlate the $B \rightarrow K^*$ results of the previous subsection with currently possible $B \rightarrow K$ measurements. We focus on the differential spectrum of $B \rightarrow Ke^+e^-$ and R_K . The relevant $B \rightarrow KV$ partial width induced by each of the operators is

$$\Gamma(B \rightarrow KV)|_{Q_{(4)}} = \frac{1}{64\pi} |C_{(4)}|^2 \frac{m_B^3}{m_V^2} \lambda^{3/2} f_+^2(m_V^2), \quad (3.12)$$

$$\Gamma(B \rightarrow KV)|_{Q_{(5)}} = \frac{1}{16\pi} \frac{|C_{(5)}|^2}{\Lambda^2} m_B m_V^2 \left(1 + \frac{m_K}{m_B}\right)^{-2} \lambda^{3/2} f_T^2(m_V^2), \quad (3.13)$$

$$\Gamma(B \rightarrow KV)|_{Q_{(6)}} = \frac{1}{64\pi} \frac{|C_{(6)}|^2}{\Lambda^4} m_B^3 m_V^2 \lambda^{3/2} f_+^2(m_V^2), \quad (3.14)$$

where now m_B denotes the B^+ mass and m_K the K^+ mass. In the kinematical function λ defined in eq. (3.11) m_{K^*} should be replaced by m_K . The $B \rightarrow K$ form factors f_+ and f_T are taken from ref. [40] (see appendix B).

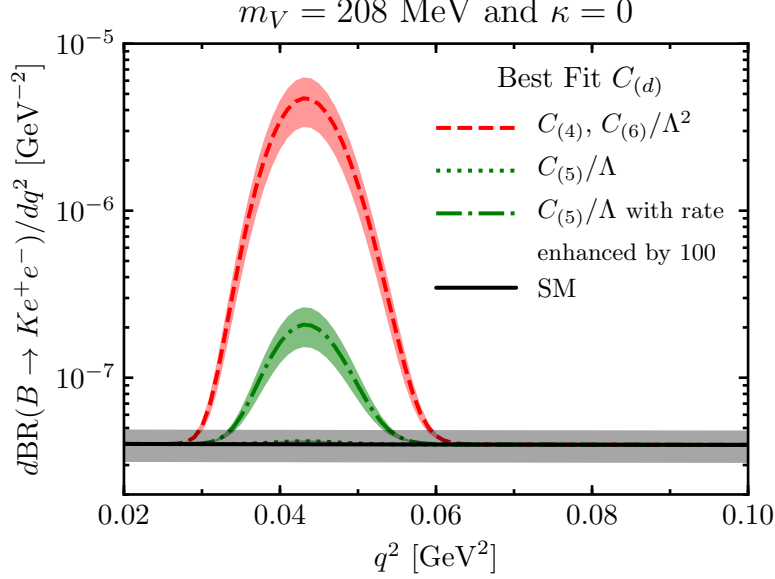


Figure 4: The differential branching ratio $d\text{BR}(B \rightarrow Ke^+e^-)/dq^2$ in the SM (solid black) and in the presence of a light vector resonance with mass 208 MeV produced via the operators $Q_{(4)}$ (dashed red), $Q_{(5)}$ (dotted green) and $Q_{(6)}$ (dashed red). In each case, we use the best-fit value for the corresponding Wilson coefficients (see table 1). The predictions for $Q_{(4)}$ and $Q_{(6)}$ are identical. The $Q_{(5)}$ peak is much less prominent. For illustration we also show this case after enhancing the NP rate by a factor of 100 (dotted dashed green).

From eqs. (3.8)–(3.10) and eqs. (3.12)–(3.14) we see that: (i) The $B \rightarrow KV$ and $B \rightarrow K^*V$ decay widths induced by $Q_{(5)}$ depend on different form factors than those induced by $Q_{(4)}/Q_{(6)}$. (ii) The $B \rightarrow KV$ and $B \rightarrow K^*V$ decay widths induced by $Q_{(5)}$ have different scaling with the vector mass m_V , while those induced by $Q_{(4)}/Q_{(6)}$ do not. Therefore, the magnitude of the peak in the $B \rightarrow K\ell^+\ell^-$ spectra can be used as a way to disentangle the two production modes of the resonance. (iii) The fact that

$$\frac{\Gamma(B \rightarrow K^*V)|_{Q_{(4)}}}{\Gamma(B \rightarrow K^*V)|_{Q_{(6)}}} = \frac{\Gamma(B \rightarrow KV)|_{Q_{(4)}}}{\Gamma(B \rightarrow KV)|_{Q_{(6)}}} \quad (3.15)$$

implies that the correlation of the $B \rightarrow K^*\ell^+\ell^-$ and $B \rightarrow K\ell^+\ell^-$ observables is identical in both production modes. Therefore, the two production modes cannot be distinguished via the $B \rightarrow K\ell^+\ell^-$ spectra or a measurement of R_K at low q^2 .

Due to the absence of the photon-pole contribution to $B \rightarrow Ke^+e^-$, a peak in the $B \rightarrow Ke^+e^-$ spectrum from the new resonance is potentially even more prominent than in $B \rightarrow K^*e^+e^-$. In fig. 4 we show the differential $\text{BR}(B \rightarrow Ke^+e^-)$ as a function of q^2 . The solid black line depicts the predicted branching ratio in the SM, computed using `flavio`. The red and green lines show the SM plus NP contribution from $Q_{(4)}/Q_{(6)}$ and $Q_{(5)}$, respectively, at the best-fit points given in table 1. The bands correspond

Dark photon, $\kappa = 0$

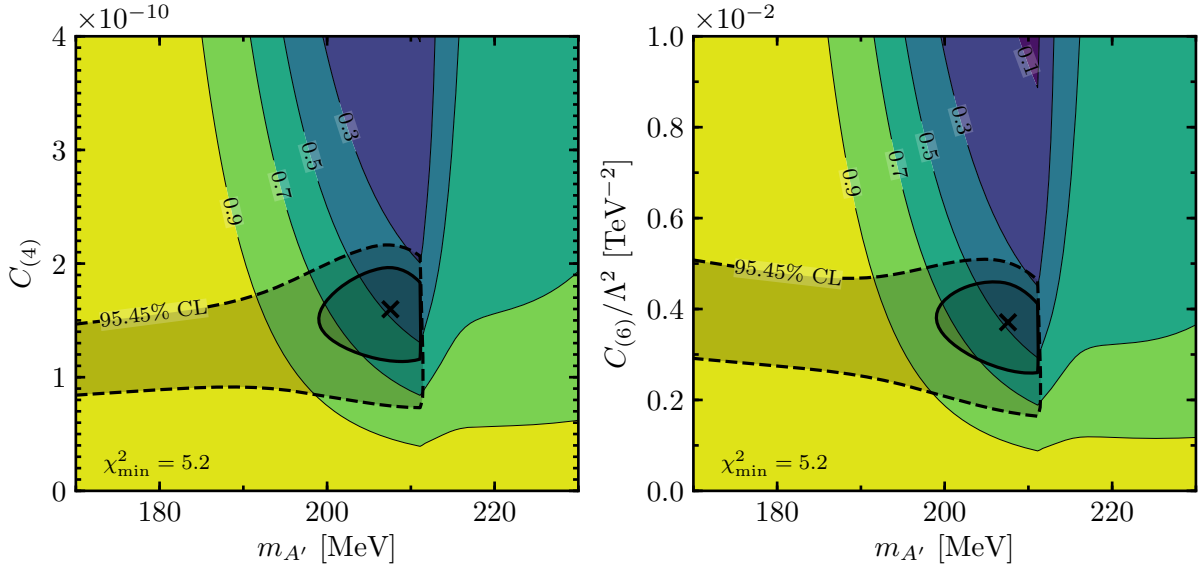


Figure 5: Values of R_K for a dark photon with $\kappa = 0$ as a function of the Wilson coefficients $C_{(4)}$ (left) and $C_{(6)}$ (right), and the dark-photon mass, $m_{A'}$. Superimposed is the best-fit region from the measurement of R_{K^*} , $B \rightarrow K^* A' (\rightarrow \mu^+ \mu^-)$ and $B \rightarrow K^* e^+ e^-$. We do not show the corresponding case for $Q_{(5)}$ because in the best-fit region the effects in R_K are unobservably small.

to the 68.27 C.L. regions of $\text{BR}(B \rightarrow K^* V)$ from the χ^2 for the case $m_V = 208 \text{ MeV}$. The prediction from $Q_{(4)}$ and $Q_{(6)}$ coincide due to eq. (3.15), which is why they are represented by the same line. While $Q_{(4)}$ and $Q_{(6)}$ yield a sizeable deviation from the SM, the contribution of $Q_{(5)}$ at the best-fit point (dotted green line) is small compared to the SM theory uncertainties (grey band). The dotted dashed green line shows the $Q_{(5)}$ contribution if the NP rate is enhanced by a factor 100 with respect to the best-fit rate. The reason for this large suppression of the dipole contribution is that the B decay into the pseudoscalar K and the vector V via $Q_{(5)}$ is suppressed by m_V^2/m_B^2 compared to the decay into the two vectors K^* and V , due to angular-momentum conservation.

In fig. 5, we consider the case of a dark photon with $\kappa = 0$. We show contours of the predicted value of R_K in a bin of $q^2 \in [0.045, 1] \text{ GeV}^2$, along with the 68.27% and 95.45% C.L. regions of the χ^2 including the constraints from $B \rightarrow K^* A' (\rightarrow \mu^+ \mu^-)$, $B \rightarrow K^* e^+ e^-$ and the measured value of R_{K^*} in the low- q^2 bin. We find that if the new resonance is produced via the operators $Q_{(4)}$ (left panel) or $Q_{(6)}$ (right panel) then R_K can be as low as ~ 0.3 in the 95.45% C.L. preferred region. If the new resonance is instead coupled via $Q_{(5)}$ then R_K is barely altered from its SM value and we do not show this case.

In fig. 6, we consider the case of an “electrophilic” vector resonance, i.e., $\text{BR}(V \rightarrow e^+ e^-) = 100\%$, and, analogously to fig. 5, show R_K contours and the preferred regions from the χ^2 . In this case, the bounds from the $B \rightarrow K^* V (\rightarrow \mu^+ \mu^-)$ resonance search do not apply and even a resonance with a mass above the di-muon threshold can account

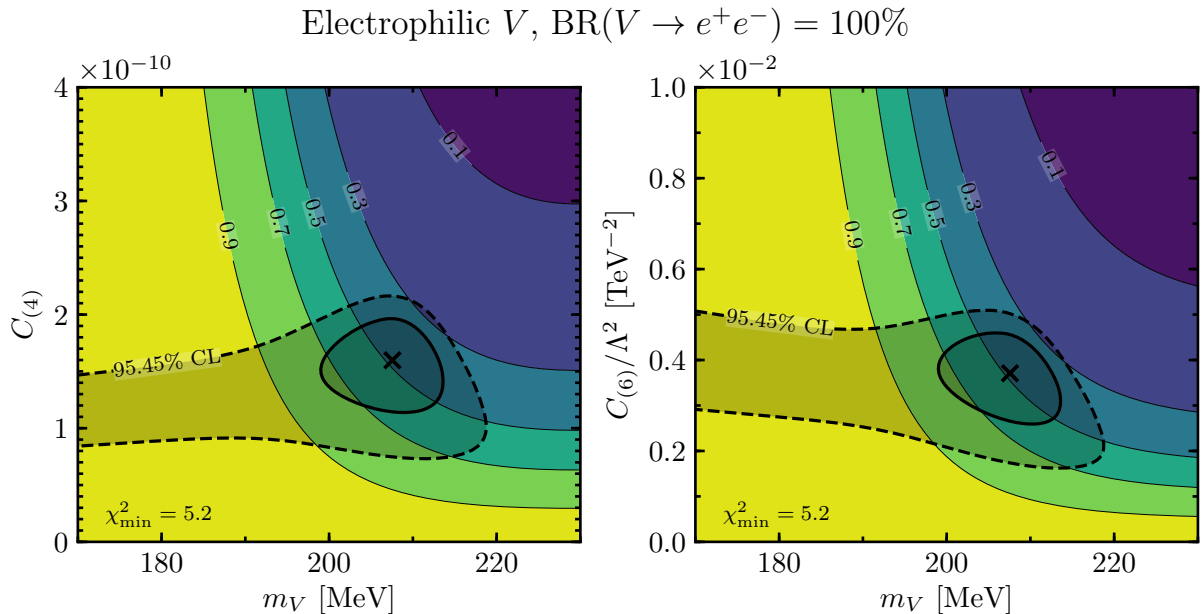


Figure 6: Values of R_K for an electrophilic V , i.e., $\text{BR}(V \rightarrow e^+e^-) = 100\%$, as a function of the Wilson coefficients $C_{(4)}$ (left) and $C_{(6)}$ (right), and the resonance mass, m_V . Superimposed is the best-fit region from the measurement of R_{K^*} and the electron distribution. We do not show the corresponding case for $Q_{(5)}$ because in the best-fit region the effects in R_K are unobservably small.

for the low- q^2 bin of R_{K^*} and significantly affect R_K .

For both the dark photon and the electrophilic case we see that, if a future measurement of R_K in such a low- q^2 bin finds a value significantly smaller than the SM expectation, the $Q_{(4)}$ and $Q_{(6)}$ production modes would be favored, while the $Q_{(5)}$ mode would be disfavored.

4 Cross-Checking Lepton-Universality Violation

The central issue looming over the subject of lepton universality in semileptonic B decays (and over NP speculations about its origin) is the question of experimental uncertainties and of possible unaccounted bias in the reconstruction of e^+e^- pairs. If the deviation in the low- q^2 bin of R_{K^*} persists in the future, and at the same time no peaks in the $B \rightarrow K^{(*)}e^+e^-$ and $B_s \rightarrow \phi e^+e^-$ spectra are observed, the case for a systematic experimental origin of the deviation would be strengthened.

The LHCb collaboration has performed detailed analyses of the leptonic decays of J/ψ . Those are known to be universal: $\text{BR}(J/\psi \rightarrow \ell^+\ell^-)$ are equal for muon and electron final states to very good accuracy [41]. Therefore, LHCb uses these resonant sources of $\ell^+\ell^-$ as a normalization for the continuum contribution in R_K and R_{K^*} . The collaboration also tests the overall consistency of the e^+e^- reconstruction using photon conversion to electrons in the $K^*\gamma$ final states of B^0 decays.

| Decay mode | BR | Semileptonic BR, $\mu^+\mu^-$ or e^+e^- | N_{decays} at 5 fb^{-1} |
|------------------------------------|---------------------|---|--|
| $D^\pm \rightarrow \pi^\pm \phi$ | $5.4 \cdot 10^{-3}$ | $1.6 \cdot 10^{-6}$ | $\mathcal{O}(10^4)$ |
| $D^0 \rightarrow \pi^+ \pi^- \phi$ | $2.6 \cdot 10^{-3}$ | $7.6 \cdot 10^{-7}$ | $\mathcal{O}(10^4)$ |
| $D_s^\pm \rightarrow \pi^\pm \phi$ | $2.5 \cdot 10^{-2}$ | $1.3 \cdot 10^{-5}$ | $\mathcal{O}(10^4)$ |
| $D_s^\pm \rightarrow K^\pm \phi$ | $1.8 \cdot 10^{-4}$ | $5.3 \cdot 10^{-8}$ | $\mathcal{O}(10^2)$ |

Table 2: Collection of D^\pm , D^0 , and D_s meson decay modes with which tests of lepton universality of the ϕ meson are possible at LHCb. The individual branching ratios are extracted using PDG tables [44], while the leptonic branching to individual flavors is obtained by multiplying with $BR(\phi \rightarrow \ell^+ \ell^-)$, which we take to be $2.9 \cdot 10^{-4}$. The estimates for the number of expected events with 5 fb^{-1} is obtained by a simple rescaling of results from ref. [43].

Here we would like to point out that additional tests can and should be made in other channels where one would not expect large deviations from lepton universality, namely in decays to hadronic final states with the lowest ϕ resonance, $m_\phi = 1020 \text{ MeV}$. The q^2 value corresponding to $\phi \rightarrow \ell^+ \ell^-$ is 1.04 GeV^2 and is, therefore, very close to the interesting values for q^2 . ϕ mesons are copiously produced in a hadronic environment and can be clearly seen as a peak in the di-muon invariant mass spectrum [42]. However, in order to have the maximum resemblance to the semileptonic B decays, one should explore the decay channels of charmed mesons that lead to charged hadrons and a ϕ , with ϕ decaying leptonically (e.g. $D^+ \rightarrow \pi^\pm \mu^\mp \mu^+$ [43]).

In table 2, we summarize the relevant decay modes of charmed mesons that can be investigated by the LHCb collaboration. Table 2 suggests that the studies of leptonic decays of ϕ generated by charmed mesons are entirely feasible given the number of expected events. We take a previous study of $D^\pm \rightarrow \pi^\pm \mu^+ \mu^-$ by LHCb, which recorded several thousand ϕ -mediated lepton pairs with 1 fb^{-1} of integrated luminosity, as an example [43] and make a simple rescaling to higher integrated luminosity to estimate the number of expected events with 5 fb^{-1} .

Unlike the case of B decays where continuum contributions are comparable to the resonant one, the hadron + $\ell^+ \ell^-$ decay modes of D mesons are dominated by resonances [43]. Therefore, *if* the suggested test would produce highly discrepant yields for lepton pairs from ϕ decays, e.g., by $\sim 30\%$ as is the case for R_K and R_{K^*} , then this would likely indicate a potential problem with the LHCb reconstruction of electron pairs. If on the other hand, the results for the ϕ -mediated $\ell^+ \ell^-$ effects come out to be flavor universal, then it would further strengthen the case for NP in R_K and R_{K^*} .

As a note of potential curiosity, the comparison of the currently most precise results for the leptonic widths of ϕ from KLOE [45] and Novosibirsk [46] already produces a mildly non-universal answer at an approximately 10% level. In particular, taking the combination of $\sqrt{\Gamma_{\phi \rightarrow ee} \times \Gamma_{\phi \rightarrow \mu\mu}}$ measured by KLOE and combining it with the

measurement of $\Gamma_{\phi \rightarrow ee}$ from Novosibirsk, we find $\text{BR}(\phi \rightarrow \mu^+\mu^-)/\text{BR}(\phi \rightarrow e^+e^-) = 1.15 \pm 0.06$. When we include all KLOE and Novosibirsk measurements of leptonic widths of ϕ the discrepancy is milder, $\text{BR}(\phi \rightarrow \mu^+\mu^-)/\text{BR}(\phi \rightarrow e^+e^-) = 1.09 \pm 0.05$.

5 Discussion and Conclusions

We explored possible NP explanations of the anomaly in the low- q^2 bin of R_{K^*} observed by LHCb. Heavy NP parameterized in terms of an effective Lagrangian typically does not affect the low- q^2 bin appreciably. We found that effects from new, light degrees of freedom can account for the observation, but are strongly constrained and an explanation of the excess is only possible in a very narrow range of parameter space. In particular, we argued that off-shell exchange of a light resonance, X , (significantly below the di-muon threshold) can be excluded as the origin of the discrepancy at low q^2 , as the implied two-body decay rate $B \rightarrow X_s X$ typically exceeds the measured total B width.

An explanation in terms of one new resonance is possible if the resonance mass is close to the di-muon threshold, $m_X \simeq 2m_\mu \simeq 211$ MeV, and if the resonance decays predominantly into electrons. Notably, in this mass range the difference of muon and electron mass are enough to trigger effects in R_{K^*} originating solely from kinematics, without requiring a lepton-flavor non-universal coupling. A simple interesting example model is given by a dark photon. To explain the low- q^2 discrepancy one needs $\text{BR}(B \rightarrow K^* A') \times \text{BR}(A' \rightarrow e^+e^-) \sim 10^{-7}$. The light resonance near the di-muon threshold affects mainly the low- q^2 bin of R_{K^*} , while its effect at higher q^2 is negligible. Additional NP is required to explain the high- q^2 bin of R_{K^*} and the anomaly in R_K .

A fairly robust model-independent implication of a light-NP origin of the low- q^2 discrepancy is a prominent peak close to the di-muon threshold in the $B \rightarrow K^* e^+ e^-$ and $B_s \rightarrow \phi e^+ e^-$ di-electron invariant-mass spectra. Within specific models, we investigated all possible couplings of a vector resonance up to dimension six. We found that couplings from dimensions-four and five operators can originate from plausible UV completions in the sense that their Wilson coefficients may be induced from perturbative NP at or above the electroweak scale. One possibility for a model for dimension-four couplings is gauged (anomalous) baryon number with a gauge coupling of order 10^{-3} . This model does not require any sources of flavor violation beyond the SM, neither in the quark nor the lepton sector. It is also notable that the scale at which the dimension-five couplings are induced in order to account for the low- q^2 R_{K^*} anomaly is compatible with the scale needed to explain its high- q^2 counterpart.

We also investigated the implications of these models for $B \rightarrow K$ data and found that the size of a corresponding peak in the $B \rightarrow K e^+ e^-$ di-electron invariant-mass spectrum depends on the nature of the flavor violating $b \rightarrow s$ coupling of the resonance. In particular, dimension-four and six interactions lead to a prominent peak in $B \rightarrow K e^+ e^-$, while the dimension-five interaction (dipole) leaves the $B \rightarrow K e^+ e^-$ decay SM-like to an excellent approximation.

If the predicted peaks are not observed in future measurements, then this would suggest that the effect is unlikely to originate from NP. In such a case, a persistent

anomaly in the low- q^2 bin could imply a systematic experimental origin of the deviation, which may also affect the interpretation of other LFU violation hints, such as the high- q^2 bins of $R_{K^{(*)}}$. Possible exotic NP explanations that would not predict a peak may still be possible. These include unparticles, or a large discrete set of resonances that are so close in mass that they cannot be resolved as peaks experimentally.

As an additional experimental cross check of LFU violation, we proposed measurements of the leptonic ϕ branching ratios at LHCb. To have the maximum resemblance to the semileptonic B decays, we suggested to explore the decay channels of charmed mesons to charged hadrons and a ϕ . We identified several D^\pm , D^0 , and D_s meson decay modes, each of which lead to $\mathcal{O}(10^4)$ leptonically decaying ϕ 's with 5 fb^{-1} of data. This suggests excellent prospects for a precise measurement of the ratio of $\phi \rightarrow \mu^+\mu^-$ and $\phi \rightarrow e^+e^-$ branching ratios.

Acknowledgements

We thank Kaladi Babu and Pedro Machado for discussions. WA and SG thank the Mainz Institute for Theoretical Physics (MITP) for its hospitality and support during parts of this work. The work of WA and SG was in part performed at the Aspen Center for Physics, which is supported by National Science Foundation grant PHY-1607611. The research of WA is supported by the National Science Foundation under Grant No. PHY-1720252. SG is supported by a National Science Foundation CAREER Grant No. PHY-1654502. MJB and AT would like to thank Fermilab for its kind hospitality and support during the early stages of this project. Fermilab is operated by Fermi Research Alliance, LLC under Contract No. DE-AC02-07CH11359 with the United States Department of Energy. MJB was supported by the German Research Foundation (DFG) under Grant Nos. KO 4820/1-1 and FOR 2239, by the European Research Council (ERC) under the European Union's Horizon 2020 research and innovation programme (grant agreement No. 637506, “ ν Directions”), by Horizon 2020 INVISIBLESplus (H2020-MSCA-RISE-2015-690575) and by the Swiss National Science Foundation (SNF) under contract 200021-175940. The work of AT was supported under the International Cooperative Research and Development Agreement for Basic Science Cooperation (CRADA No. FRA-2016-0040) between Fermilab and Johannes Gutenberg University Mainz, and partially by the Advanced Grant EFT4LHC of the European Research Council (ERC) and the Cluster of Excellence Precision Physics, Fundamental Interactions and Structure of Matter (PRISMA – EXC 1098).

A Light Off-Shell V in $b \rightarrow s\ell\ell$

In this appendix we demonstrate that the measured value of R_{K^*} in the low- q^2 bin cannot be explained by the off-shell exchange of a light vector boson, V , with vectorial couplings to leptons and a mass significantly below the di-muon threshold. Such a light vector could in principle lead to a NP effect in the three-body decay $B \rightarrow K^*\ell^+\ell^-$

that is enhanced at low q^2 by m_B^2/q^2 . In practice, however, we find that such an effect is severely constrained by limits on the partial width of the inclusive two-body decay $B \rightarrow X_s V$ and limits on the couplings of V to leptons.

A robust limit on the $B \rightarrow X_s V$ partial width, which is completely independent of the possible V decay modes, is given by the measured total B width, $\Gamma(B \rightarrow X_s V) < 1/\tau_B$. An equally robust and slightly stronger constraint can be obtained from measurements of the charm yield per B meson decay. The BaBar analysis [47] finds that the average number of charm quarks per B^- decay is $N_c^- = 0.968_{-0.043}^{+0.045}$, where we added the statistical uncertainty, the systematic uncertainty, and the uncertainty from charm branching ratios in quadrature. The measured value of N_c^- implies that the branching ratios of non-standard charmless decay modes such as $B \rightarrow X_s V$ are bounded by 11.8% at the 2σ level. It follows that

$$\Gamma(B \rightarrow X_s V) \lesssim 11.8\% \times 1/\tau_B \simeq 4.7 \cdot 10^{-14} \text{ GeV} , \quad (\text{A.1})$$

where we used the lifetime of the charged B^\pm meson $\tau_B = 1.638 \pm 0.004 \text{ ps}$ [44]. We note that in many cases *much* stronger bounds on the $B \rightarrow X_s V$ branching ratio can be obtained depending on the V decay modes. If the V decays dominantly to invisible final states or is stable on detector scales, constraints from $B \rightarrow K^{(*)} \bar{\nu} \nu$ imply $\text{BR}(B \rightarrow KV) \lesssim 1.7 \cdot 10^{-5}$ [27] and $\text{BR}(B \rightarrow K^* V) \lesssim 4.0 \cdot 10^{-5}$ [26] at 90% C.L. Constraints at a similar level can be derived from $B \rightarrow K^{(*)} e^+ e^-$ measurements [19, 48], if the V decays promptly into electrons and has a mass $m_V \gtrsim 20 \text{ MeV}$. We will not consider these much stronger constraints in the following, as the model-independent constraint in eq. (A.1) turns out to be sufficiently powerful to exclude observable effects in the low- q^2 bin of R_{K^*} .

In eq. (3.1) we introduced the possible flavor violating interactions of a new vector to SM quarks up to dimension six. The contribution of the dimension-six interaction, $Q_{(6)}^{(\prime)}$, to $B \rightarrow K^* \ell^+ \ell^-$ are not enhanced at low q^2 by m_B^2/q^2 , and we, therefore, only consider $Q_{(4)}$ and $Q_{(5)}$ in the following. In the limit $m_V \ll m_B$, we find the following partial decay widths of the inclusive decay $B \rightarrow X_s V$

$$\Gamma(B \rightarrow X_s V)|_{Q_{(4)}} = \frac{|C_{(4)}|^2 m_b^3}{32\pi m_V^2}, \quad \Gamma(B \rightarrow X_s V)|_{Q_{(5)}} = \frac{|C_{(5)}|^2 m_b^3}{4\pi \Lambda^2}. \quad (\text{A.2})$$

Using eq. (A.1) and the PDG value for the bottom pole mass $m_b = 4.78 \pm 0.06 \text{ GeV}$ [44], we find the following bounds on the couplings $C_{(4)}$ and $C_{(5)}$

$$|C_{(4)}| \lesssim \left(\frac{m_V}{100 \text{ MeV}} \right) \times 2.1 \cdot 10^{-8}, \quad \frac{|C_{(5)}|}{\Lambda} \lesssim 7.4 \cdot 10^{-8} \text{ GeV}^{-1}. \quad (\text{A.3})$$

The off-shell corrections to the low- q^2 bin of R_{K^*} do not only depend on the quark flavor violating couplings of the V , but also on the V couplings to muons and electrons. Here we focus on vector couplings⁸

$$\mathcal{L}_{\text{leptons}} \supset g_e (\bar{e} \gamma^\nu e) V_\nu + g_\mu (\bar{\mu} \gamma^\nu \mu) V_\nu . \quad (\text{A.4})$$

⁸ Introducing simultaneously axial-vector couplings and/or couplings from higher-dimensional operators may open up the possibility of tuned cancellations in some of the constraints discussed below. We do not consider the possibility of such cancellations here.

Two concrete setups that induce such vector couplings are: (i) kinetic mixing of V with the photon; (ii) the gauging of flavor-specific lepton number. In the case of kinetic mixing, one has $g_e = g_\mu$. In the case of gauged lepton number, one simultaneously also generates couplings to the corresponding neutrinos. In the latter case, strong constraints on the coupling to muons, g_μ , can be derived from the measured rate of neutrino trident production [49]. The bound is at the level of $g_\mu \lesssim 10^{-3}$ and is shown in the left panel of fig. 7. This bound is independent of the decay modes of the V . Also shown in the plot is the region of parameter space that would allow us to address the $(g-2)_\mu$ anomaly at the 2σ level, as well as the exclusion by $(g-2)_\mu$ at the 5σ level. The $(g-2)_\mu$ bound is independent of both the V decay modes and the couplings to neutrinos.

The anomalous magnetic moment of the electron, $(g-2)_e$, leads to a bound on the V coupling to electrons that is independent of the V decay modes. The anomaly in the gyromagnetic ratio of the electron, $a_e = \frac{1}{2}(g-2)_e$, can be predicted in the SM with high precision using measurements of the fine-structure constant in atomic physics experiments. This results in the bound [50]

$$|\Delta a_e| \lesssim 8.1 \cdot 10^{-13} . \quad (\text{A.5})$$

The contribution to a_e from a V loop implies a bound on the coupling g_e

$$\Delta a_e \simeq \frac{g_e^2}{12\pi^2} \frac{m_e^2}{m_V^2} \Rightarrow g_e \lesssim \left(\frac{m_V}{100 \text{ MeV}} \right) \times 1.9 \cdot 10^{-3} , \quad (\text{A.6})$$

where we assumed $m_V \gg m_e$. Additional strong constraints on the coupling to electrons can be obtained from the fixed target experiment NA64 [51] and from BaBar searches [31, 52]. In the relevant range of V masses and couplings, there are only two possible decay modes of V : (i) the coupling g_e allows the V to decay promptly to electrons; (ii) V can decay invisibly into neutrinos or a light dark sector. If invisible decays are absent or negligibly small, the BaBar search for dark photons [31] leads to constraints on g_e that are stronger than the constraints from $(g-2)_e$ for masses $m_V \gtrsim 20$ MeV. In the central panel of fig. 7 we show both constraints. If the invisible decays dominate, the BaBar mono-photon search [52] and the NA64 search for dark photons [51] lead to strong constraints on g_e as summarized in the right panel of fig. 7. Finally, if V also has couplings to quarks (as in the dark-photon case) additional constraints become relevant that restrict the parameter space further [29].

In fig. 8 we show the maximal effects in the low- q^2 bin of R_{K^*} that can be induced by the off-shell exchange of a light vector as function of the vector mass taking into account the constraints on the couplings to quarks and leptons discussed above. We consider separately the production from $Q_{(4)}$ and $Q_{(5)}$, taking their Wilson coefficients to saturate the bounds in eq. (A.3). To identify the maximal effect in R_{K^*} we vary the sign of the Wilson coefficients and the phase difference between the SM and the NP contribution. In the left panel, we consider a muophilic case in which V couples solely to muon flavor. For a given V mass we take the maximally allowed g_μ coupling from the ν -trident bound (left panel of fig. 7). In the central panel, we consider an electrophilic case in which V decays solely to electrons. For a given V mass we take the maximally allowed g_e coupling

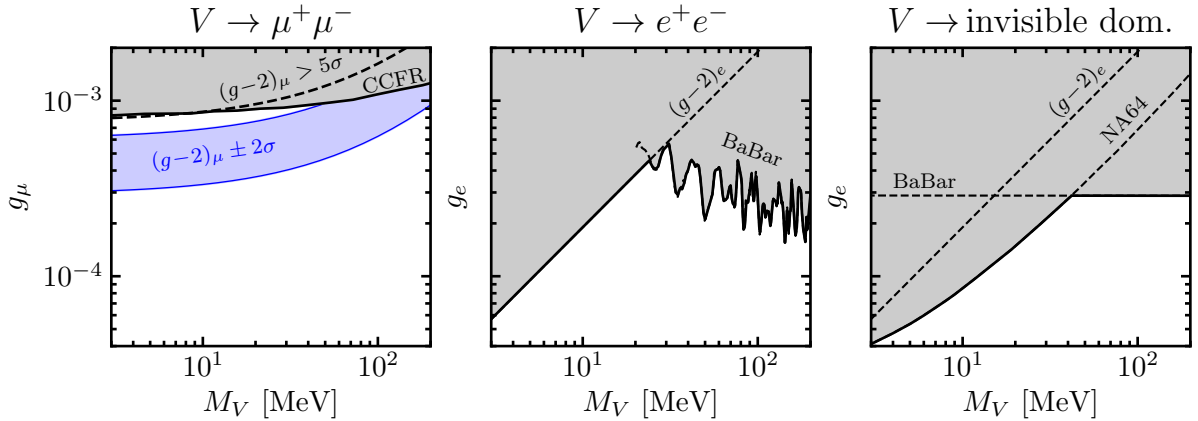


Figure 7: Bounds on the vector couplings of a light vector, V , to muons (left) and electrons (center and right) as a function of the vector mass. On the left panel, the constraints from ν -trident production based on measurements by the CCFR collaboration do not apply in models in which V does not couple to neutrinos, i.e., dark-photon models. The central plot assumes the absence of a relevant invisible decay rate of the vector. The right plot assumes that the invisible decays dominate.

from the combination of the bounds in the central panel of fig. 7. In the right panel, we consider the case in which V can decay to electrons but primarily decays invisibly. For a given V mass we take the maximally allowed g_e coupling from the combination of the bounds in the right panel of fig. 7. For each case, we show the maximal value of $R_{K^*}^{[0.045,1.1]}|_{\text{SM}} - R_{K^*}^{[0.045,1.1]}|_{Q(d)}$ as a function of the V mass. We find that the effects are much smaller than the current discrepancy $R_{K^*}^{[0.045,1.1]}|_{\text{SM}} - R_{K^*}^{[0.045,1.1]}|_{\text{LHCb}} = 0.25^{+0.11}_{-0.08}$ (horizontal green band).

B Form Factors

For the computation of the decay width $\Gamma(B \rightarrow K^{(*)}V)$ we use the form factors given in refs. [39, 40]. In the limit of vanishing momentum transfer, $q^2 \rightarrow 0$, the relevant $B \rightarrow K^*$ form factors are

$$\begin{aligned} V(0) &= 0.341 \pm 0.036, & A_1(0) &= 0.269 \pm 0.029, & A_3(0) &= 0.356 \pm 0.046, \\ T_1(0) = T_2(0) &= 0.282 \pm 0.031, & T_3(0) &= 0.180 \pm 0.039, \end{aligned} \quad (\text{B.1})$$

and for the relevant $B \rightarrow K$ form factors

$$f_+(0) = 0.335 \pm 0.036, \quad f_T(0) = 0.279 \pm 0.067. \quad (\text{B.2})$$

None of these form factors change appreciably between $q^2 = 0$ and $q^2 = m_V^2 \sim 4m_\mu^2$. In our numerics we thus use the zero-momentum transfer values above.

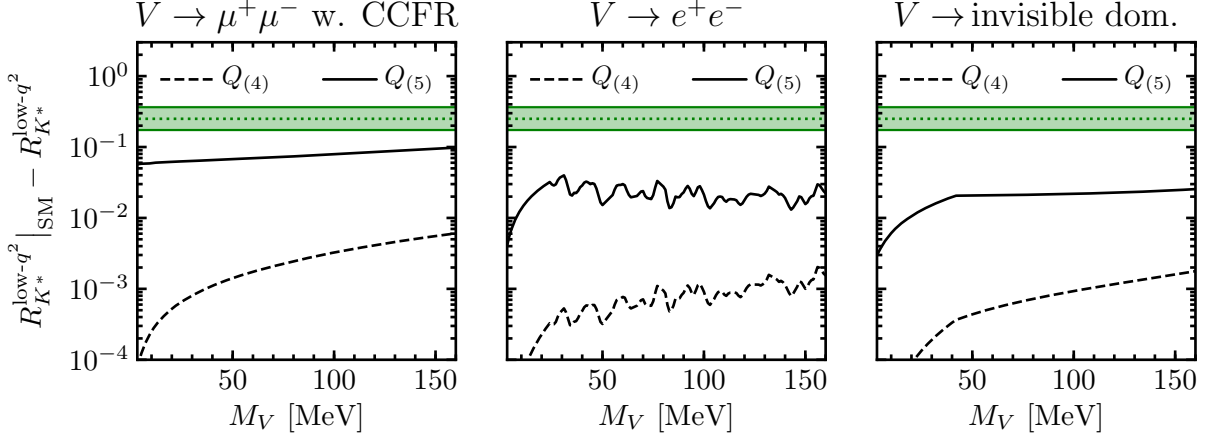


Figure 8: Maximal effects from $Q_{(4)}$ and $Q_{(5)}$ in the low- q^2 bin of R_{K^*} from the off-shell exchange of a light vector, V , as function of the vector mass. In the left panel, V decays solely to muons with a coupling that saturates the ν -trident bound from the left panel of fig. 7. In the central panel, V decays solely to electrons with a coupling saturating the bounds in the central panel of fig. 7. In the right panel, V couples to electrons but primarily decays invisibly, the maximally allowed coupling to electrons is plotted in the right panel of fig. 7. For each case, we show the maximal value of $R_{K^*}^{[0.045,1.1]}|_{SM} - R_{K^*}^{[0.045,1.1]}|_{Q(d)}$ as a function of the V mass. We see that the effects are much smaller than the current discrepancy (horizontal green band).

The functions \mathcal{F}_1 and \mathcal{F}_2 in eqs. (3.8), (3.9), and (3.10) are given in terms of form factors by

$$\begin{aligned}
\mathcal{F}_1(x, y) = & + V^2 2xy(1 - \sqrt{x})^2 (x^2 - 2x(1 + y) + (1 - y)^2) \\
& + A_1^2 \frac{y}{4} (1 + \sqrt{x})^2 (-2(3x + 1)y^2 + (3x + 1)^2 y + 8(x - 1)^2 x + y^3) \\
& + A_3^2 x (x^2 - 2x(1 + y) + (1 - y)^2)^2 \\
& + A_1 A_3 (1 + \sqrt{x}) \sqrt{xy} (3x - y + 1) (x^2 - 2x(1 + y) + (1 - y)^2) ,
\end{aligned} \tag{B.3}$$

$$\begin{aligned}
\mathcal{F}_2(x, y) = & + T_1^2 8x(1 - x)^2 (x^2 - 2x(1 + y) + (1 - y)^2) \\
& + T_2^2 (1 - x)^2 (-2(3x + 1)y^2 + (3x + 1)^2 y + 8(x - 1)^2 x + y^3) \\
& + T_3^2 y (x^2 - 2x(1 + y) + (1 - y)^2)^2 \\
& + T_2 T_3 2(x - 1)y(3x - y + 1) (x^2 - 2x(1 + y) + (1 - y)^2) .
\end{aligned} \tag{B.4}$$

References

- [1] **LHCb** Collaboration, R. Aaij *et al.*, “Test of lepton universality using $B^+ \rightarrow K^+ \ell^+ \ell^-$ decays,” *Phys. Rev. Lett.* **113** (2014) 151601, [arXiv:1406.6482](#) [hep-ex].

- [2] **LHCb** Collaboration, R. Aaij *et al.*, “Test of lepton universality with $B^0 \rightarrow K^{*0} \ell^+ \ell^-$ decays,” *JHEP* **08** (2017) 055, [arXiv:1705.05802 \[hep-ex\]](#).
- [3] G. Hiller and F. Kruger, “More model-independent analysis of $b \rightarrow s$ processes,” *Phys. Rev.* **D69** (2004) 074020, [arXiv:hep-ph/0310219 \[hep-ph\]](#).
- [4] M. Bordone, G. Isidori, and A. Pattori, “On the Standard Model predictions for R_K and R_{K^*} ,” *Eur. Phys. J.* **C76** no. 8, (2016) 440, [arXiv:1605.07633 \[hep-ph\]](#).
- [5] W. Altmannshofer, P. Stangl, and D. M. Straub, “Interpreting Hints for Lepton Flavor Universality Violation,” *Phys. Rev.* **D96** no. 5, (2017) 055008, [arXiv:1704.05435 \[hep-ph\]](#).
- [6] B. Capdevila, A. Crivellin, S. Descotes-Genon, J. Matias, and J. Virto, “Patterns of New Physics in $b \rightarrow s \ell^+ \ell^-$ transitions in the light of recent data,” [arXiv:1704.05340 \[hep-ph\]](#).
- [7] G. D’Amico, M. Nardecchia, P. Panci, F. Sannino, A. Strumia, R. Torre, and A. Urbano, “Flavour anomalies after the R_{K^*} measurement,” *JHEP* **09** (2017) 010, [arXiv:1704.05438 \[hep-ph\]](#).
- [8] L.-S. Geng, B. Grinstein, S. Jäger, J. Martin Camalich, X.-L. Ren, and R.-X. Shi, “Towards the discovery of new physics with lepton-universality ratios of $b \rightarrow s \ell \ell$ decays,” [arXiv:1704.05446 \[hep-ph\]](#).
- [9] M. Ciuchini, A. M. Coutinho, M. Fedele, E. Franco, A. Paul, L. Silvestrini, and M. Valli, “On Flavourful Easter eggs for New Physics hunger and Lepton Flavour Universality violation,” *Eur. Phys. J.* **C77** no. 10, (2017) 688, [arXiv:1704.05447 \[hep-ph\]](#).
- [10] D. Bardhan, P. Byakti, and D. Ghosh, “Role of Tensor operators in R_K and R_{K^*} ,” *Phys. Lett.* **B773** (2017) 505–512, [arXiv:1705.09305 \[hep-ph\]](#).
- [11] K. Fuyuto, W.-S. Hou, and M. Kohda, “ Z' -induced FCNC decays of top, beauty, and strange quarks,” *Phys. Rev.* **D93** no. 5, (2016) 054021, [arXiv:1512.09026 \[hep-ph\]](#).
- [12] A. Datta, J. Liao, and D. Marfatia, “A light Z' for the R_K puzzle and nonstandard neutrino interactions,” *Phys. Lett.* **B768** (2017) 265–269, [arXiv:1702.01099 \[hep-ph\]](#).
- [13] F. Sala and D. M. Straub, “A New Light Particle in B Decays?,” [arXiv:1704.06188 \[hep-ph\]](#).
- [14] D. Ghosh, “Explaining the R_K and R_{K^*} anomalies,” [arXiv:1704.06240 \[hep-ph\]](#).

- [15] A. K. Alok, B. Bhattacharya, A. Datta, D. Kumar, J. Kumar, and D. London, “New Physics in $b \rightarrow s\mu^+\mu^-$ after the Measurement of R_{K^*} ,” [arXiv:1704.07397 \[hep-ph\]](#).
- [16] F. Bishara, U. Haisch, and P. F. Monni, “Regarding light resonance interpretations of the B decay anomalies,” *Phys. Rev.* **D96** no. 5, (2017) 055002, [arXiv:1705.03465 \[hep-ph\]](#).
- [17] A. Datta, J. Kumar, J. Liao, and D. Marfatia, “New light mediators for the R_K and R_{K^*} puzzles,” [arXiv:1705.08423 \[hep-ph\]](#).
- [18] K. S. Babu, A. Friedland, P. A. N. Machado, and I. Mocioiu, “Flavor Gauge Models Below the Fermi Scale,” [arXiv:1705.01822 \[hep-ph\]](#).
- [19] **LHCb** Collaboration, R. Aaij *et al.*, “Angular analysis of the $B^0 \rightarrow K^{*0}e^+e^-$ decay in the low- q^2 region,” *JHEP* **04** (2015) 064, [arXiv:1501.03038 \[hep-ex\]](#).
- [20] **LHCb** Collaboration, R. Aaij *et al.*, “Search for hidden-sector bosons in $B^0 \rightarrow K^{*0}\mu^+\mu^-$ decays,” *Phys. Rev. Lett.* **115** no. 16, (2015) 161802, [arXiv:1508.04094 \[hep-ex\]](#).
- [21] Y. Amhis *et al.*, “Averages of b -hadron, c -hadron, and τ -lepton properties as of summer 2016,” [arXiv:1612.07233 \[hep-ex\]](#).
- [22] M. Pepe Altarelli and F. Teubert, “ B Physics at LHCb,” *Int. J. Mod. Phys.* **A23** (2008) 5117–5136, [arXiv:0802.1901 \[hep-ph\]](#).
- [23] P. Ilten, J. Thaler, M. Williams, and W. Xue, “Dark photons from charm mesons at LHCb,” *Phys. Rev.* **D92** no. 11, (2015) 115017, [arXiv:1509.06765 \[hep-ph\]](#).
- [24] **LHCb** Collaboration, R. Aaij *et al.*, “LHCb Detector Performance,” *Int. J. Mod. Phys.* **A30** no. 07, (2015) 1530022, [arXiv:1412.6352 \[hep-ex\]](#).
- [25] D. M. Straub, “Flavio,” 2017. [https://flav-io.github.io/\[doi:10.5281/zenodo.555949\]](https://flav-io.github.io/[doi:10.5281/zenodo.555949]).
- [26] **Belle** Collaboration, O. Lutz *et al.*, “Search for $B \rightarrow h^{(*)}\nu\bar{\nu}$ with the full Belle $\Upsilon(4S)$ data sample,” *Phys. Rev.* **D87** no. 11, (2013) 111103, [arXiv:1303.3719 \[hep-ex\]](#).
- [27] **BaBar** Collaboration, J. P. Lees *et al.*, “Search for $B \rightarrow K^{(*)}\nu\bar{\nu}$ and invisible quarkonium decays,” *Phys. Rev.* **D87** no. 11, (2013) 112005, [arXiv:1303.7465 \[hep-ex\]](#).
- [28] **APEX** Collaboration, S. Abrahamyan *et al.*, “Search for a New Gauge Boson in Electron-Nucleus Fixed-Target Scattering by the APEX Experiment,” *Phys. Rev. Lett.* **107** (2011) 191804, [arXiv:1108.2750 \[hep-ex\]](#).

- [29] R. Essig *et al.*, “Working Group Report: New Light Weakly Coupled Particles,” in *Proceedings, 2013 Community Summer Study on the Future of U.S. Particle Physics: Snowmass on the Mississippi (CSS2013): Minneapolis, MN, USA, July 29-August 6, 2013*. 2013. [arXiv:1311.0029](https://arxiv.org/abs/1311.0029) [hep-ph].
<http://inspirehep.net/record/1263039/files/arXiv:1311.0029.pdf>.
- [30] H. Merkel *et al.*, “Search at the Mainz Microtron for Light Massive Gauge Bosons Relevant for the Muon $g - 2$ Anomaly,” *Phys. Rev. Lett.* **112** no. 22, (2014) 221802, [arXiv:1404.5502](https://arxiv.org/abs/1404.5502) [hep-ex].
- [31] **BaBar** Collaboration, J. P. Lees *et al.*, “Search for a Dark Photon in e^+e^- Collisions at BaBar,” *Phys. Rev. Lett.* **113** no. 20, (2014) 201801, [arXiv:1406.2980](https://arxiv.org/abs/1406.2980) [hep-ex].
- [32] J. Alexander *et al.*, “Dark Sectors 2016 Workshop: Community Report,” 2016. [arXiv:1608.08632](https://arxiv.org/abs/1608.08632) [hep-ph].
<http://inspirehep.net/record/1484628/files/arXiv:1608.08632.pdf>.
- [33] **HyperCP** Collaboration, H. Park *et al.*, “Evidence for the decay $\Sigma^+ \rightarrow p\mu^+\mu^-$,” *Phys. Rev. Lett.* **94** (2005) 021801, [arXiv:hep-ex/0501014](https://arxiv.org/abs/hep-ex/0501014) [hep-ex].
- [34] **LHCb** Collaboration, T. L. Collaboration, “Evidence for the rare decay $\Sigma^+ \rightarrow p\mu^+\mu^-$,” 2016. <http://inspirehep.net/record/1508988/files/LHCb-CONF-2016-013.pdf>.
- [35] J. A. Dror, R. Lasenby, and M. Pospelov, “New constraints on light vectors coupled to anomalous currents,” *Phys. Rev. Lett.* **119** no. 14, (2017) 141803, [arXiv:1705.06726](https://arxiv.org/abs/1705.06726) [hep-ph].
- [36] J. A. Dror, R. Lasenby, and M. Pospelov, “Dark forces coupled to nonconserved currents,” *Phys. Rev.* **D96** no. 7, (2017) 075036, [arXiv:1707.01503](https://arxiv.org/abs/1707.01503) [hep-ph].
- [37] P. J. Fox, J. Liu, D. Tucker-Smith, and N. Weiner, “An Effective Z' ,” *Phys. Rev.* **D84** (2011) 115006, [arXiv:1104.4127](https://arxiv.org/abs/1104.4127) [hep-ph].
- [38] W. Altmannshofer, S. Gori, M. Pospelov, and I. Yavin, “Quark flavor transitions in $L_\mu - L_\tau$ models,” *Phys. Rev.* **D89** (2014) 095033, [arXiv:1403.1269](https://arxiv.org/abs/1403.1269) [hep-ph].
- [39] A. Bharucha, D. M. Straub, and R. Zwicky, “ $B \rightarrow V\ell^+\ell^-$ in the Standard Model from light-cone sum rules,” *JHEP* **08** (2016) 098, [arXiv:1503.05534](https://arxiv.org/abs/1503.05534) [hep-ph].
- [40] J. A. Bailey *et al.*, “ $B \rightarrow Kl^+\ell^-$ decay form factors from three-flavor lattice QCD,” *Phys. Rev.* **D93** no. 2, (2016) 025026, [arXiv:1509.06235](https://arxiv.org/abs/1509.06235) [hep-lat].
- [41] **BESIII** Collaboration, M. Ablikim *et al.*, “Precision Measurements of $\mathcal{B}[\psi(3686) \rightarrow \pi^+\pi^-J/\psi]$ and $\mathcal{B}[J/\psi \rightarrow l^+l^-]$,” *Phys. Rev.* **D88** no. 3, (2013) 032007, [arXiv:1307.1189](https://arxiv.org/abs/1307.1189) [hep-ex].

- [42] **LHCb** Collaboration, T. L. Collaboration, “LHCb dimuon and charm mass distributions,”.
- [43] **LHCb** Collaboration, R. Aaij *et al.*, “Search for $D_{(s)}^+ \rightarrow \pi^+ \mu^+ \mu^-$ and $D_{(s)}^+ \rightarrow \pi^- \mu^+ \mu^+$ decays,” *Phys. Lett.* **B724** (2013) 203–212, [arXiv:1304.6365 \[hep-ex\]](#).
- [44] **Particle Data Group** Collaboration, C. Patrignani *et al.*, “Review of Particle Physics,” *Chin. Phys.* **C40** no. 10, (2016) 100001.
- [45] **KLOE** Collaboration, F. Ambrosino *et al.*, “Measurement of the leptonic decay widths of the phi-meson with the KLOE detector,” *Phys. Lett.* **B608** (2005) 199–205, [arXiv:hep-ex/0411082 \[hep-ex\]](#).
- [46] R. R. Akhmetshin *et al.*, “Measurement of $\phi(1020)$ meson leptonic width with CMD-2 detector at VEPP-2M Collider,” *Phys. Lett.* **B695** (2011) 412–418, [arXiv:1010.4878 \[hep-ex\]](#).
- [47] **BaBar** Collaboration, B. Aubert *et al.*, “Study of inclusive B^- and \bar{B}^0 decays to flavor-tagged D , D_s and Λ_c^+ ,” *Phys. Rev.* **D75** (2007) 072002, [arXiv:hep-ex/0606026 \[hep-ex\]](#).
- [48] **LHCb** Collaboration, R. Aaij *et al.*, “Measurement of the $B^0 \rightarrow K^{*0} e^+ e^-$ branching fraction at low dilepton mass,” *JHEP* **05** (2013) 159, [arXiv:1304.3035 \[hep-ex\]](#).
- [49] W. Altmannshofer, S. Gori, M. Pospelov, and I. Yavin, “Neutrino Trident Production: A Powerful Probe of New Physics with Neutrino Beams,” *Phys. Rev. Lett.* **113** (2014) 091801, [arXiv:1406.2332 \[hep-ph\]](#).
- [50] W. Altmannshofer, J. Brod, and M. Schmaltz, “Experimental constraints on the coupling of the Higgs boson to electrons,” *JHEP* **05** (2015) 125, [arXiv:1503.04830 \[hep-ph\]](#).
- [51] **NA64** Collaboration, D. Banerjee *et al.*, “Search for invisible decays of sub-GeV dark photons in missing-energy events at the CERN SPS,” *Phys. Rev. Lett.* **118** no. 1, (2017) 011802, [arXiv:1610.02988 \[hep-ex\]](#).
- [52] **BaBar** Collaboration, J. P. Lees *et al.*, “Search for invisible decays of a dark photon produced in e^+e^- collisions at BaBar,” [arXiv:1702.03327 \[hep-ex\]](#).